JGR Space Physics

RESEARCH ARTICLE
10.1029/2020JA027934

On the 2015 St. Patrick's Storm Turbulent State of the Ionosphere: Hints From the Swarm Mission

P. De Michelis[1], A. Pignalberi[1], G. Consolini[2], I. Coco[1], R. Tozzi[1], M. Pezzopane[1], F. Giannattasio[1], and G. Balasis[3]

[1]Istituto Nazionale di Geofisica e Vulcanologia, Rome, Italy, [2]INAF-Istituto di Astrofisica e Planetologia Spaziali, Rome, Italy, [3]IAASARS-National Observatory of Athens, Athens, Greece

Key Points:
- Self-similarity/affinity nature of the plasma density fluctuations in the *F* region of middle- and high-latitude ionosphere
- Plasma density fluctuations at high latitudes in the auroral and polar cap regions seem to be related to a turbulent ionospheric dynamics
- High values of RODI can be a proxy of the occurrence of ionospheric turbulence

Correspondence to:
P. De Michelis,
paola.demichelis@ingv.it

Citation:
De Michelis, P., Pignalberi, A., Consolini, G., Coco, I., Tozzi, R., & Pezzopane, M., et al. (2020). On the 2015 St. Patrick's storm turbulent state of the ionosphere: Hints from the Swarm mission. *Journal of Geophysical Research: Space Physics*, *125*, e2020JA027934. https://doi.org/10.1029/2020JA027934

Received 20 FEB 2020
Accepted 12 JUN 2020
Accepted article online 3 JUL 2020

Abstract The scaling features of electron density fluctuations during the St. Patrick's magnetic storm (17 March 2015) are analyzed to try to characterize the possible turbulent nature of the ionosphere during the development of the geomagnetic storm. The electron density values recorded by two of the three satellites of Swarm constellation during a period of 7 days (16–22 March 2015) around the storm peak are analyzed at middle- and high-latitude regions in both hemispheres. The analysis reveals interesting patterns in the scaling properties of electron density fluctuations and a possible explanation for the occurrence of high values of the Rate of change Of the electron Density Index (RODI). Indeed, the obtained results seem to suggest that very high values of RODI, which describes the structuring of the plasma within a fixed time and is used as an ionospheric disturbance index, are correlated with the antipersistent character of electron density fluctuations and with the values around 5/3 of the power spectral density scaling exponent. These features are independent of the different phases of the analyzed geomagnetic storm and seem to support the idea of a fluid and/or magnetohydrodynamic turbulence as the main responsible of the high values of RODI recorded at high latitudes in the auroral and polar cap regions.

Plain Language Summary Electron density fluctuations characterizing the ionospheric plasma during the St. Patrick's geomagnetic storm occurred on 17 March 2015 are analyzed to investigate their possible turbulent nature. To perform this study, electron density values recorded by two of the three satellites of the Swarm constellation are considered at middle and high latitudes of both hemispheres between 16 and 22 March 2015. Results show that electron density fluctuations present interesting patterns and that high values of the Rate Of change of electron Density Index (RODI), which is used as an ionospheric disturbance index, may be related to a turbulent dynamics of the ionosphere. Specifically, independently of the different phases of the analyzed geomagnetic storm, the observed features seem to support the idea of a fluid and/or magnetohydrodynamic turbulence as the main cause of the high values of RODI recorded at high latitudes in the auroral and polar cap regions.

1. Introduction

Turbulence phenomena are at the origin of several important ionospheric dynamical processes. They usually happen as a result of the coupling processes, which characterize the solar wind-magnetosphere-ionosphere system and can significantly affect both the ionospheric plasma dynamics and the energization of ionospheric particles. Consequently, the dynamics of physical quantities like electron and ion densities, velocities and temperatures, and magnetic and electric fields, can display fluctuations occurring on many spatial and temporal scales, among which a nonlinear transfer of energy can occur.

One of the first review papers focusing on the ionospheric plasma turbulence is the one published in the mid-eighties by Kintner and Seyler (1985), which proposes and discusses different theories and models on turbulence mechanisms, capable of explaining particular behaviors shown in the ionosphere by both the electron density and the electric field. Beyond this interesting review, it should be stressed, however, that in the years many other papers have been published on the occurrence of turbulence processes in the ionosphere. For example, a great attention has been given to the turbulent properties of electric (see, e.g., Golovchanskaya & Kozelov, 2010; Heppner et al., 1993; Kozelov & Golovchanskaya, 2006; Tam et al., 2005; Weimer et al., 1985) and magnetic fluctuations (De Michelis et al., 2015; Golovchanskaya et al., 2006; Kozelov & Golovchanskaya, 2006) observed at different altitudes and latitudes by ground and space. The

increased interest in the ionospheric turbulence phenomena (e.g., De Michelis et al., 2017; Dyrud et al., 2008; Grach et al., 2016; Pécseli, 2016; Spicher et al., 2015) demonstrates the need to better understand these processes and the different ways in which they can influence the ionospheric environment. For instance, the generation and dynamics of ionospheric inhomogeneities and irregularities (see, e.g., Basu et al., 1988; Earle et al., 1989; Giannattasio et al., 2019) can be affected by turbulence processes occurring in the plasma and this means that ionospheric turbulence may play a significant role in the framework of space weather. Indeed, the ionospheric inhomogeneities and irregularities are among the main causes of disturbances in the propagation of electromagnetic signals in the ionosphere and consequently a better understanding of the turbulence will be of help to all those systems, such as the Global Positioning Systems (GPS) and Global Navigation Satellite Systems (GNSS), which are based on the propagation of an electromagnetic signals through the ionosphere.

Ionosondes, incoherent scatter radars, VHF/HF coherent backscatter radars, all-sky cameras, and GPS stations are usually used to investigate ionospheric irregularities. However, these ground-based measuring facilities, which permit a good investigation of irregularities in the bottomside of the ionosphere, do not permit a good investigation of the topside ionospheric irregularities where in situ observations can be more useful. These can be obtained using instruments on-board of low-Earth-orbit (LEO) satellites. Thus, a good opportunity to unveil how turbulence affects the ionospheric environment, in generating multiscale plasma structures and plasma inhomogenities, comes from the analysis of the nature of fluctuations and their multiscaling features of the electron density estimated by data as recorded by the European Space Agency (ESA) Swarm mission.

The Swarm constellation was launched in November 2013 to provide high-quality measurements of Earth's magnetic field and associated plasma environment (Olsen et al., 2013). These three identical satellites, which fly in polar orbit at two different altitudes of about 450 km (Swarm A and Swarm C) and 510 km (Swarm B), explore the *F* region of the ionosphere through the measurements of a vector fluxgate, an absolute scalar magnetometers, and the electric field instrument (EFI), which includes Langmuir Probes (LPs) and a Thermal Ion Imager for measuring plasma density and temperature (Knudsen et al., 2017).

It is evident that data recorded on-board LEO satellites give the opportunity to study the ionospheric irregularities at different latitudinal regions. Here, we focus on middle- and high-latitude regions of both hemispheres. Indeed, while for the equatorial regions there have been a number of experimental studies accompanied with analytical models, there has been a much slower progress about studies of the high-latitude ionospheric plasma irregularities associated with instabilities and turbulence. This is in part due to difficult accessibility of these regions and to the complex dynamics of the ionospheric plasma at high latitudes.

Among some recent papers on high-latitude plasma density irregularities, Spicher et al. (2015) have clearly shown how nonlinear wave interactions and coherent mode coupling might play a relevant role in generating electron density fluctuations at the edge of the polar cap, while in the region where electron precipitation is dominant, the fluctuations associated with a plasma enhancement are mainly characterized by a more random nature. All these findings suggest that a clear link between particle precipitation and turbulent-like structures exists in these regions. To analyze the ionospheric plasma irregularities and turbulence, a common approach is to study the power spectra of the electron density responsible for these irregularities and, in particular, their slopes, which could give information on the possible mechanism through which these irregularities are generated. In the high-latitude *F* region the analysis of the power spectra of plasma density fluctuations in the range of scales between several kilometers and tens of meters shows that spectra are often characterized by a power law with a spectral index around −1.8 (e.g., Basu et al., 1984; Dyson et al., 1974; Mounir et al., 1991). This suggests that the generation of plasma irregularities in the ionospheric polar regions could be associated with the gradient drift instability (e.g., Cerisier et al., 1985; Mounir et al., 1991) or with the Kelvin-Helmholtz instability (Basu et al., 1988; Kintner & Seyler, 1985).

In this work data recorded on-board Swarm satellites are used to get information about the turbulent nature of the ionospheric plasma at middle and high latitudes in both hemispheres by analyzing the scaling features of small-scale fluctuations of the electron density recorded during the St. Patrick's geomagnetic storm of March 2015, the well-known St. Patrick's event. It was the strongest geomagnetic storm of the 24th solar cycle that reached the G4 level on the National Oceanic and Atmospheric Administration (NOAA) scale (Poppe, 2000). It was characterized by an intense particle precipitation in the polar regions that generated

both an enhancement in substorm activity and the occurrence of intense ionospheric irregularities during the main and recovery phases of the geomagnetic storm (Cherniak et al., 2015). This geomagnetic storm has been extensively investigated in the scientific community, for example, analyzing the ionospheric effects on global scale (Astafyeva et al., 2015), on the equatorial latitudes of the Indian and nearby regions (Ram et al., 2015; Ramsingh et al., 2015), on middle and low latitudes (Balasis et al., 2018; Nava et al., 2016). We analyze this event from a completely different point of view. The main aims are indeed (1) to analyze the daily patterns of the scaling properties of electron density fluctuations during the development of this geomagnetic storm and (2) to investigate a possible relation between them and the occurrence of plasma density irregularities as described by the Rate Of change of electron Density Index (the so-called RODI) (Jin et al., 2019). The main idea proposed by this work is to try to understand if there is a correlation between RODI and the scaling/spectral features of electron density fluctuations and so if RODI can be used as a proxy for the occurrence of ionospheric plasma turbulence.

Indeed, RODI obtained by measurements made on-board Swarm constellation, is a measure of the occurrence of irregularities at the Swarm altitude. So, it would be potentially able to give us information about the nature of ionospheric irregularities achieved at the same altitude. This would give an additional importance to an index, well known and used in the scientific community, born as a simple measure of the electron density irregularities and able to identify their presence but not their nature.

2. Data and Processing Approach

The present work focuses on the analysis of the fluctuations of in situ electron density provided by the LPs on-board Swarm satellites during the geomagnetic storm occurred on 17 March 2015. Level 1b electron density data at a rate of 1 Hz for two of the three Swarm satellites (A and B) have been selected from the ESA ftp repository (https://earth.esa.int/web/guest/swarm/data-access) for a time window of 7 days from 16 to 22 March 2015. According to the "Swarm Level 1b Product Definition" document (available at https://earth.esa.int/web/guest/document-library/browse-document-library/-/article/swarm-level-1b-product-definition), we have excluded data flagged as "non nominal" (parameters Flags_Ne and Flags_Te different from either 10 or 20). Then, all data gaps resulting either from flag selection or from data unavailability have been filled by "not-a-number" values, in order to guarantee the continuity of the time series.

Data are presented in terms of Quasi-Dipole (QD) latitude (Laundal & Richmond, 2016) and magnetic local time (MLT) coordinates and reported in polar view daily maps in both hemispheres (from 50° to the magnetic pole). In each map, magnetic noon is at the top and magnetic midnight is at the bottom.

Figure 1 shows polar daily maps of the electron density for the Northern Hemisphere covering the selected time interval. These maps, obtained considering the measurements coming from Swarm A and Swarm B, are reported together with the temporal trend of two different geomagnetic indices, SYM-H and AE, which well describe the geomagnetic activity in the middle- and high-latitude regions during the selected period. These indices allow to following the temporal evolution of the disturbance of the geomagnetic field recorded on the ground mainly due to an increase of the magnetospheric ring current and an intense particle precipitation at high latitudes, which cause a substorm activity enhancement. Due to orbital features, during the analyzed period Swarm A and B span two different magnetic local time intervals (06:00-9:00 and 18:00–21:00 MLT, respectively) as it is evident in Figure 1. The same data daily polar maps are drawn for the case of the Southern Hemisphere in Figure 2. The comparison between Figures 1 and 2 shows the different spatial extent of data in the two hemispheres, which is due to the different distance of the magnetic poles from the geographic ones. Polar daily maps of electron density show a well-known feature characterizing disturbed conditions that is a significant electron density decrease due to compositional changes (Prölss, 1987).

The in situ electron density data have been used to evaluate RODI, which is the standard deviation of the Rate of change Of electron Density (ROD) in a sliding window of fixed size. This index has been evaluated according to Jin et al. (2019) and considering a sliding window of 10 s. RODI polar daily maps in QD latitude versus MLT coordinates are also reported in Figures 1 and 2 for the Northern and Southern Hemispheres, respectively. From a preliminary inspection of RODI spatial distributions, we may note how the higher values of RODI ($> 3 \times 10^3$ cm^{-3} s^{-1}) are mainly located in the polar cap roughly along the noon-midnight sectors, while the auroral oval region seems to be associated with values of RODI $< 3 \times 10^3$ cm^{-3} s^{-1}. This

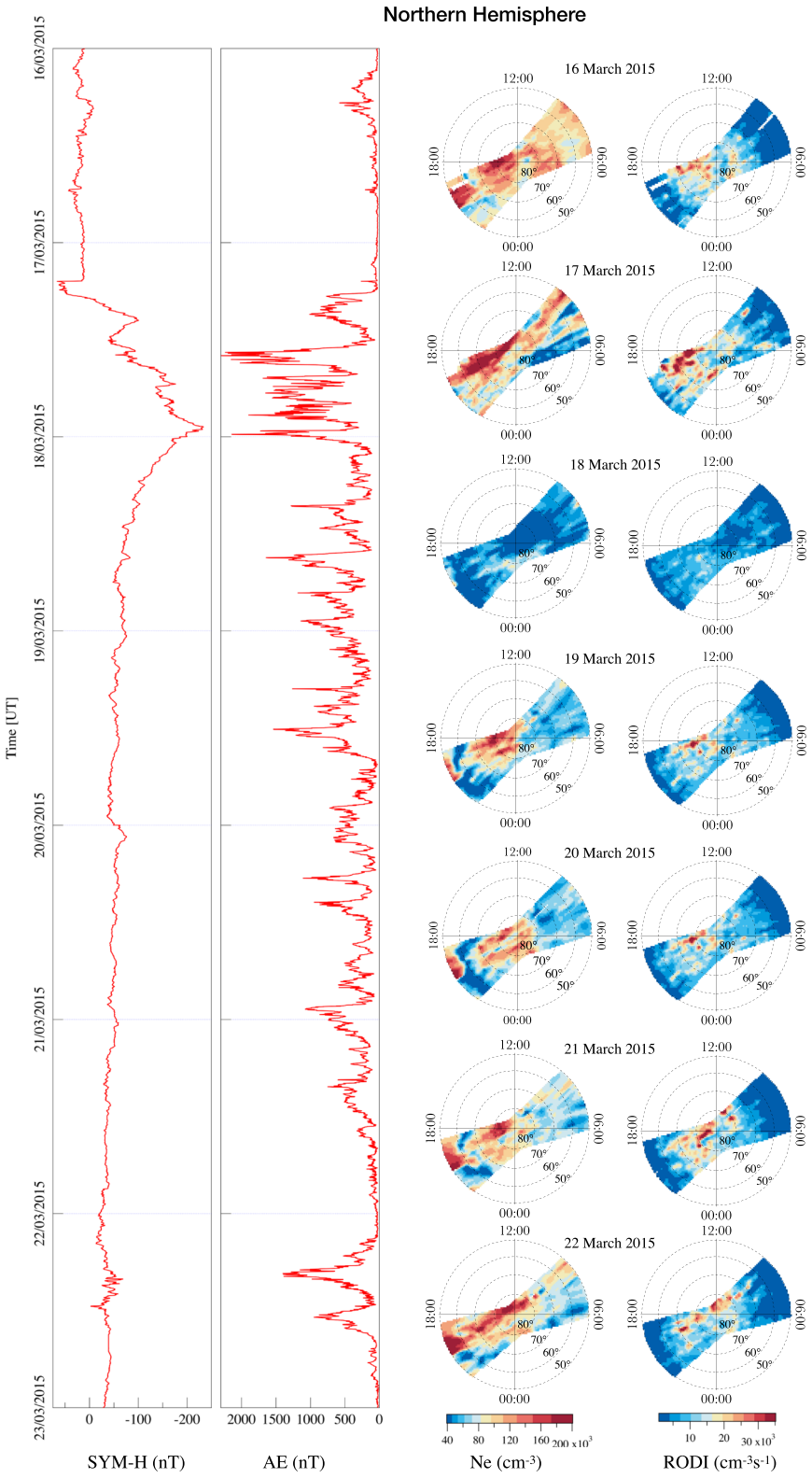

Figure 1. Daily maps of the electron density and RODI in the Northern Hemisphere during the selected time interval (16–22 March 2015) for Swarm A and B. Maps are in QD-latitude and MLT coordinate system. In each map, magnetic noon is at the top and magnetic midnight is at the bottom. The concentric circles represent contours of magnetic latitude, separated by intervals of 10°. The two panels on the left report corresponding values of geomagnetic indices SYM-H and AE.

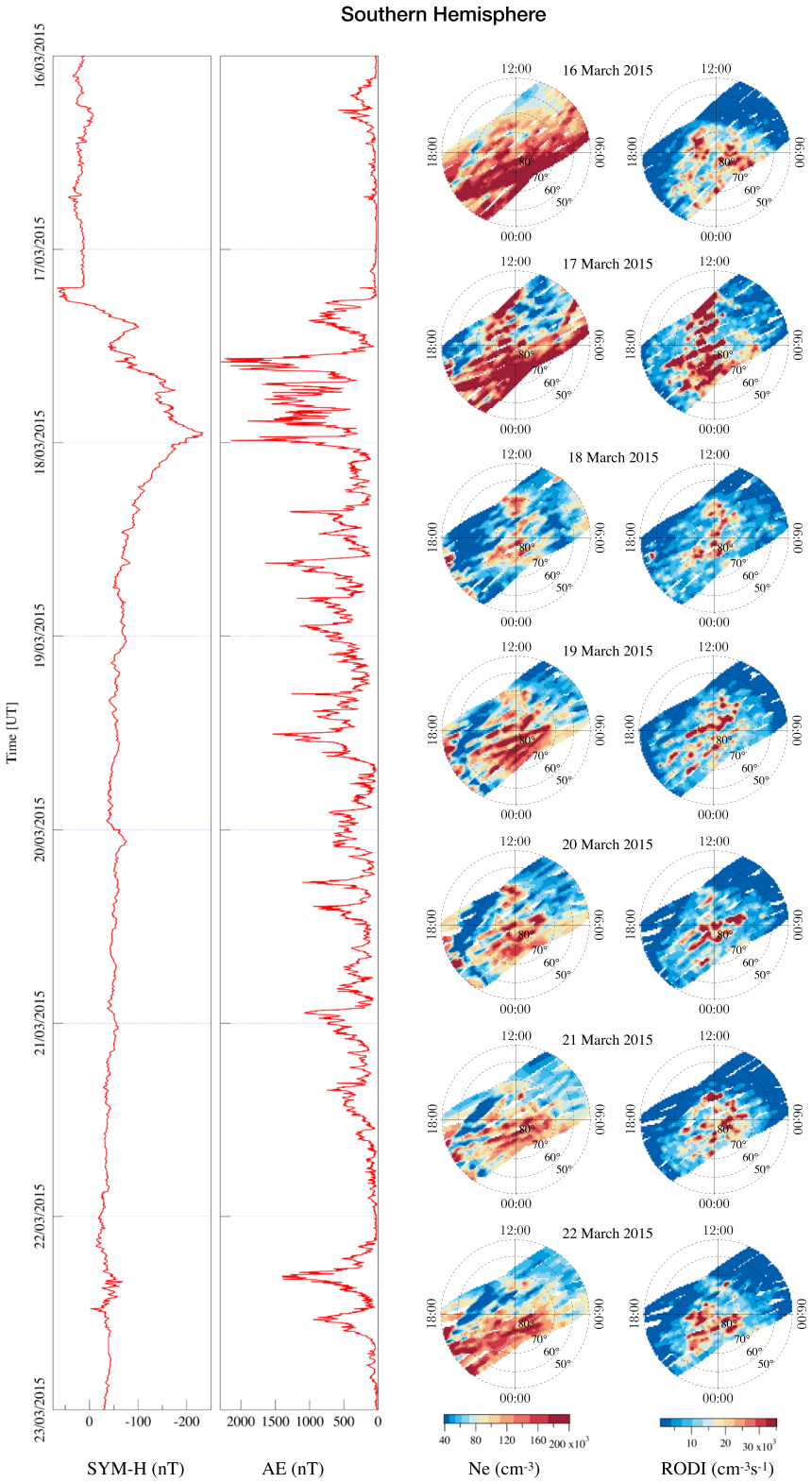

Figure 2. Daily maps of the electron density and RODI in the Southern Hemisphere during the selected time interval (16–22 March 2015) for Swarm A and B. Maps are in QD-latitude and MLT coordinate system. In each map, magnetic noon is at the top and magnetic midnight is at the bottom. The concentric circles represent contours of magnetic latitude, separated by intervals of 10°. The two panels on the left report corresponding values of geomagnetic indices SYM-H and AE.

could be a relevant aspect to be compared with the average scaling features in the two regions. We will return on this point later in the next sections.

By comparing Figures 1 and 2, no important north-south asymmetry is visible: neither in electron density and RODI patterns nor in their temporal evolution during the geomagnetic storm. The only differences are in the intensity of the variation of electron density and RODI that is slightly more intense in the Southern Hemisphere than in the Northern one, and in a partial different location of the higher RODI values on 17 March. We notice that in both hemispheres the period of the most intense irregularity occurrence corresponds with the main phase of the geomagnetic storm (occurred on 17 March 2015) when the position of the irregularities is within an oval around 60° QD-Lat. That is clearly visible in the Southern Hemisphere. During the recovery phase of the storm the region characterized by the occurrence of irregularities tends to shrink in both hemispheres. Indeed, the equatorward expansion of zone characterized by irregularity stops with the beginning of the recovery phase of the storm when the high values of RODI are mainly confined in an oval within 65–70° QD-Lat. An interesting signature of the irregularity pattern can be recognized in both hemispheres, that is, the strongest and most pronounced irregularities, that is, the highest values of RODI, are oriented in the day-night direction across the polar cap. The irregularities along this direction are stronger than those occurring along the auroral border. This means that the gradients of the ionospheric electron density induced by this geomagnetic storm were related both to auroral particle precipitation (on the auroral border) and to plasma large-scale convective motions (in the day-night direction). Indeed, the radial structure of the ionospheric irregularities have been associated mainly with the convection pattern antisunward across the polar cap of the electron density gradients (Cherniak et al., 2015; Cherniak & Zakharenkova, 2016) and not to the auroral particle precipitation.

3. Data Analysis

To investigate the scaling features of the electron density fluctuations we investigate the self-similarity/affinity nature of the measured time series using the qth-order structure function $S_q(\ell)$ for different scales (ℓ). This method consists in evaluating the scaling features of the moments of the signal increments at different spatial scales. Here, we computed the so-called generalized structure functions of the electron density that means to compute the qth-order structure functions as a function of the time delay τ, that is,

$$S_q(\tau) = \langle |N_e(t+\tau) - N_e(t)|^q \rangle, \tag{1}$$

where N_e is the electron density, t is the time, τ is the time delay, and $\langle ... \rangle$ stands for a statistical average. For a scaling process, a power law behavior is expected, that is,

$$S_q(\tau) = \tau^{\xi(q)}, \tag{2}$$

where $\xi(q)$ are the scaling exponents of the structure functions. In the case of simple fractal signals these exponents are expected to be a linear function of the moment order q, while in the case of more complex fractal signals they show a departure from such a linear dependence.

Among the hierarchy of scaling exponents $\xi(q)$ the scaling exponents of order $q = 1$ and 2 can be very useful to quantify some specific features of the signal under investigation. The first-order scaling exponent $\xi(1)$, also known as *Hurst/Hölder exponent H* (Hurst, 1956), quantifies the self-affine features of the signal and, in particular, the persistence or antipersistent character of the increments. H is a measure of the signal "roughness." A signal, whose scaling features are characterized by a Hurst exponent value less than 0.5 (H<0.5), shows an antipersistent character of its increments (a higher roughness than a random Gaussian Brownian motion), while a signal, whose scaling features are characterized by a Hurst exponent value greater than 0.5 ($H > 0.5$), shows a persistent character of its increments (Balasis et al., 2006). In other words, long-range correlated signals are characterized by a sign persistence of its increments ($H > 0.5$), while in the case of antipersistent increments (H<0.5) we talk about short-range correlated signals. Furthermore, the second-order scaling exponent $\xi(2)$ is capable of providing an information on the signal spectral features via the Wiener-Khinchin theorem. It links the spectral features to the Fourier transform of the autocorrelation function, to which the second-order structure function is directly related. In particular, in the case of a temporal signal $f(t)$ displaying scaling features characterized by a scaling

exponent $\xi(2)$ for the second-order structure function, the power spectral density (PSD) is expected to satisfy the following power law:

$$PSD(f) \sim f^{-\beta}, \tag{3}$$

where

$$\beta = \xi(2) + 1. \tag{4}$$

Thus, the investigation of scaling features of the second-order structure function can provide information on the spectral features. In passing, we note that in the case of a homogeneous fractal signal the second-order scaling exponent, $\xi(2)$, is linearly related to the first one, that is, $\xi(2) = c\,\xi(1)$, being c a constant. Deviation from this linear scaling can be associated with the occurrence of anomalous scaling features, that is, with a multifractal structure of the signal increments.

The study of scaling features may require to adopt some precautions in the case of real signals for which it is not possible to assume that some specific conditions are satisfied. Indeed, while for simple mathematical signals the scaling features are generally global, for real signals these properties can acquire a local character due to their inherent spatiotemporal nonstationarity. This is what happens in the case of satellite observations because satellites cross different regions observing physical situations that can change in space and time. To approach the study of these kind of observations, it is necessary to find reliable methods capable of evaluating the local scaling features in the different regions explored by satellites along their orbits and under different geomagnetic and interplanetary conditions. The very irregular character of the original Swarm data, which is a consequence of the strong inhomogeneity of the ionospheric plasma regions crossed by the satellites, suggests to use a local structure function method to compute their scaling features from signal increments (see, e.g., De Michelis et al., 2015, and references therein). Indeed, in this case, methods based on detrending approaches and fluctuation field analyses (Alessio et al., 2002; Carbone et al., 2004; Peng et al., 1994) could turn out to be inadequate, providing controversial results that are strongly dependent on the detrending procedure. This has been tested over a wide set of surrogated fractional, fractal, and multifractional time series, which evidenced how to our purposes the use of a local structure function method returns the best results in terms of local estimation (error less than 10%).

The structure function analysis is commonly used to analyze turbulent fields on a global scale so that, in order to apply this method locally, we need to implement it on overlapping moving windows and to remove possible large-scale variations that can affect a correct estimation of the scaling features. This is the approach of the detrended structure function analysis proposed by De Michelis et al. (2015). This method is based on three steps. Let $f(t)$ be a time series evenly sampled at fixed time intervals and $f_N(t)$ a portion of it falling in a window whose size is of N points. The first step of the method consists in locally detrending the $f_N(t)$ portion of the signal by using a polynomial function $p_N^k(t)$ of order k, defining a detrended function $g_N(t)$ as follows:

$$g_N(t) = f_N(t) - p_N^k(t). \tag{5}$$

The polynomial function is estimated by means of the traditional least squares method. As a second step, the usual structure function analysis is applied, that is, the scaling features are computed studying the scaling properties of the qth-order structure function, $S_q(\tau)$, defined on the detrended function $g_N(t)$, as follows:

$$S_q(\tau) = \langle |g_N(t+\tau) - g_N(t)|^q \rangle \sim \tau^{\xi(q)}. \tag{6}$$

Here $\xi(q)$ are the scaling exponents, where $\xi(1) \equiv H$. The maximum moment order q_m that can be locally evaluated depends on the size of the moving window, which should be at least of 10^{q_m} points, being q_m the maximum moment order. Regarding the choice of the degree k of the polynomial used to locally detrend the times series, we simply remove a linear trend on the selected time window.

The third step consists in defining the dimension of the moving window. Generally, a good window size is such that N is at least 1 order of magnitude larger than the number of points corresponding to the maximum scale to investigate. Recalling that we are using 1 Hz data, this means that if we want to study the scaling

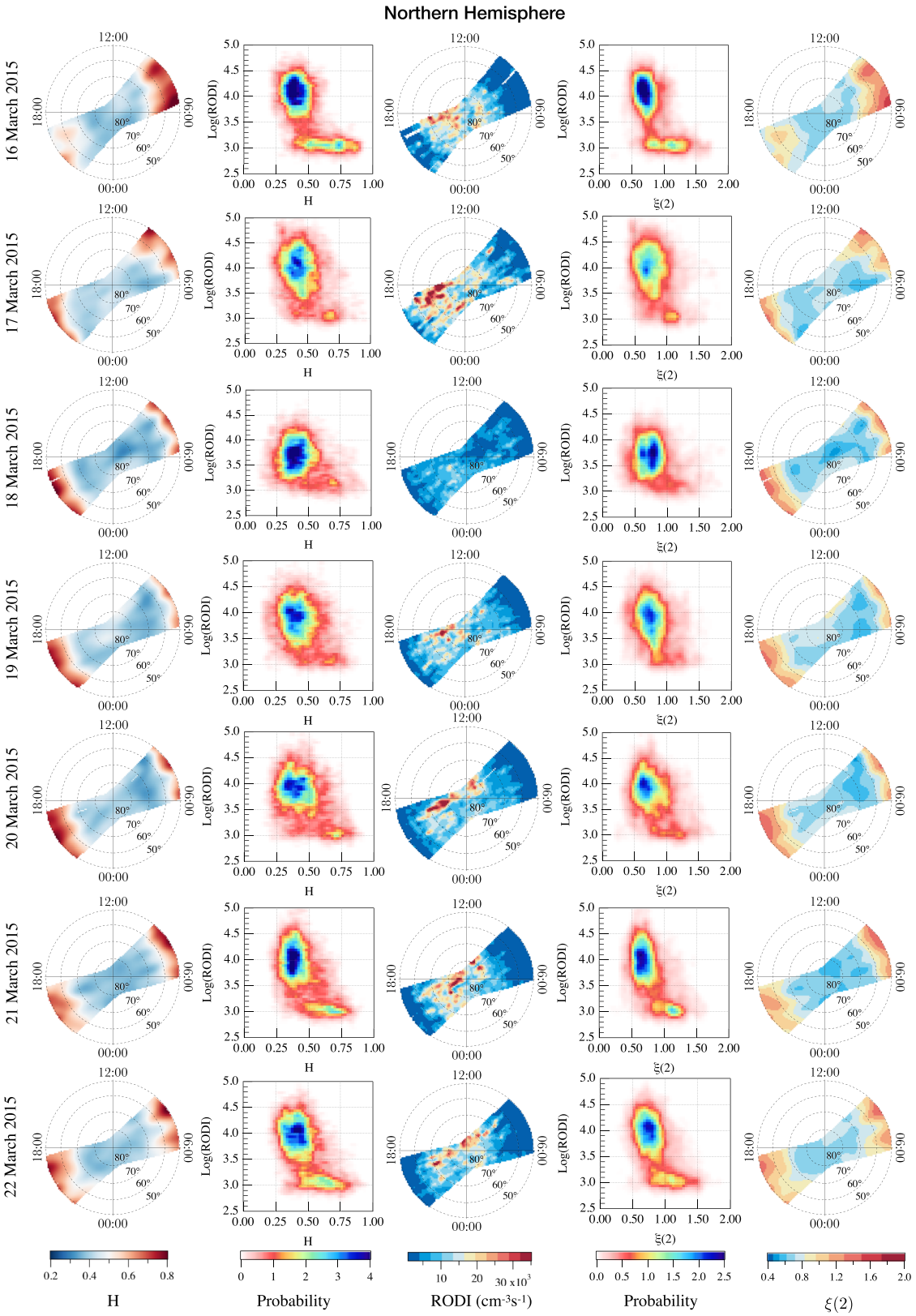

Figure 3. From the left daily maps of first-order scaling exponent, joint probability distribution between the first-order scaling exponent and RODI, RODI, joint probability distribution between the second-order scaling exponent and RODI, and the second-order scaling exponent. These daily maps cover the time interval 16–22 March 2015 (from top to bottom) in the Northern Hemisphere and are in QD-latitude and MLT coordinate system.

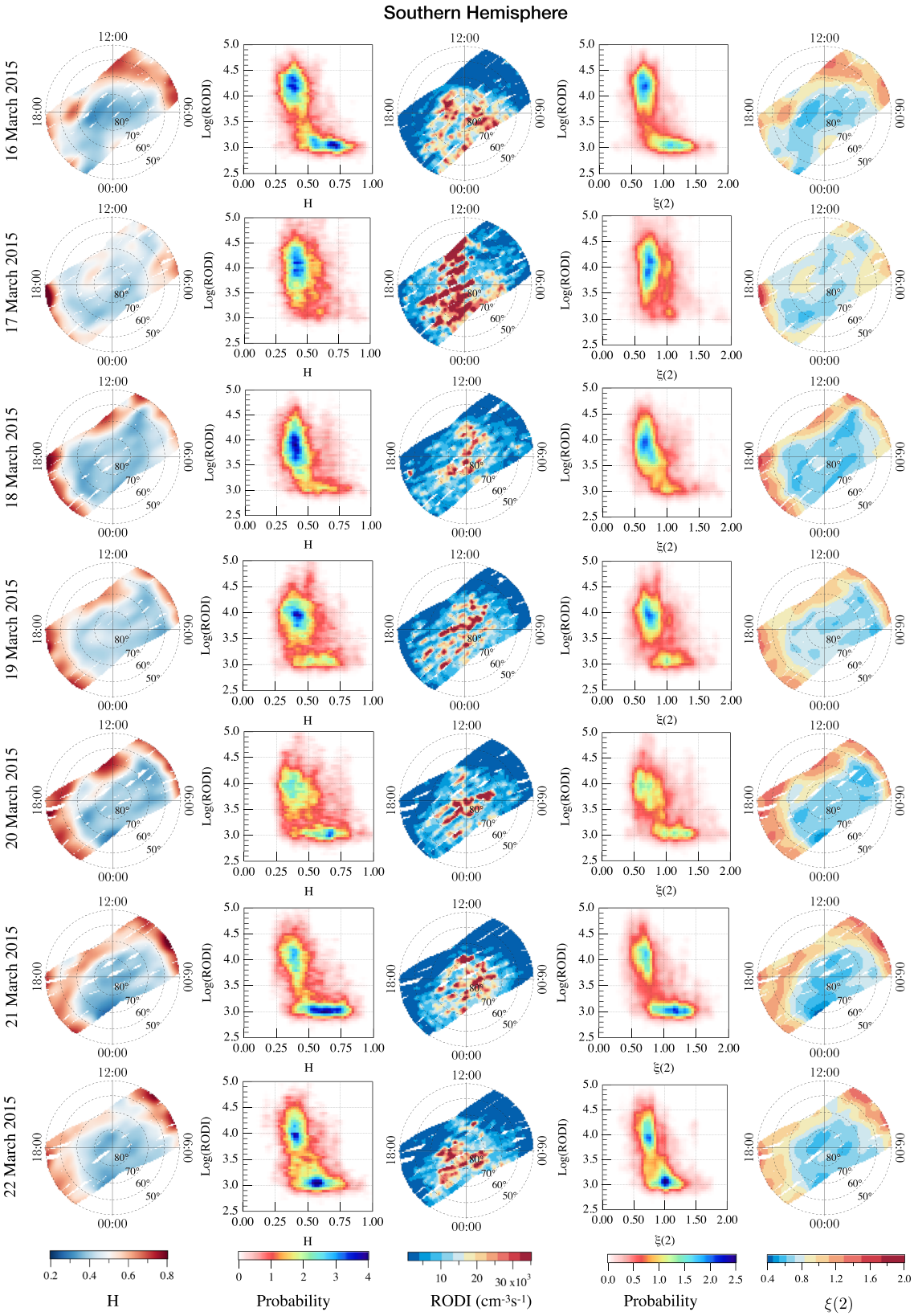

Figure 4. From the left daily maps of first-order scaling exponent, joint probability distribution between the first-order scaling exponent and RODI, RODI, joint probability distribution between the second-order scaling exponent and RODI, and the second-order scaling exponent. These daily maps cover the time interval 16–22 March 2015 (from top to bottom) in the Southern Hemisphere and are in QD-latitude and MLT coordinate system.

features in a range of scales from 1 s up to τ, the expected number of points that define the width of the moving window should be of the order of $N \sim 10\tau$. In our case, we consider $N = 301$ that means a moving window of 301 s. Detrended structure function analysis is applied in this window that is then shifted of 1 point, that is, 1 s. An accurate error analysis on surrogated data has clearly shown that error on local estimation of the scaling exponents is $\leq$10%. The time scales (τ) between 1 and 40 s are analyzed, and the estimated values of the first and second scaling exponents are associated with the position of the satellite in the instant of time that corresponds to the center of the considered time window. We suppose that the results obtained in the time domain are also valid in the spatial one. The idea is that the temporal scales can be related to the spatial scales and consequently, taking into account the orbital velocity of Swarm satellite (~7.6 km/s), the range of fluctuation scales τ corresponds to the range of spatial fluctuations between ~8 and ~250 km. This hypothesis is based on the fact that the observed low-frequency temporal electron density fluctuations in the satellite reference frame are dominated primarily by Doppler-shifted, and essentially stationary, spatial variations of the electron density structures. Thus, the time scale τ and frequency f may be viewed essentially as spatial scale $\delta \sim v_{sp}\tau$ and mode number $k \sim 2\pi f/v_{sp}$ with v_{sp} being the spacecraft velocity (e.g., Chaston, 2008; Kintner & Seyler, 1985, and references therein). On the other hand, the range of investigated timescales (from 1 up to 40 s) includes time intervals where it can be reasonably assumed that the structures are mainly frozen, as also reported in some previous papers (e.g., De Michelis et al., 2017; Gjerloev et al., 2011), where it was clearly shown that in the dayside/nightside sectors structures are nearly stable up to 60/160 s, respectively.

To limit a considerable loss of points as the consequence of the moving window approach, we analyze a single time series (electron density values) of 604,800 (number of values recorded per day (86,400) multiplied by the number of considered day (7)) points for each satellite, so the new time series relative to the first and second scaling exponents have only 300 points less than the original one. Clearly, data refer to the entire globe and to the entire time interval, therefore a selection of the values in the areas of interest, as well as for the day of interest, is necessary. For this reason, the entire time series of the selected time interval is divided into daily subsets and for each subset the first and second scaling exponents values obtained considering Swarm A and B observations during their crossings of the Northern and Southern Hemispheres are considered, simultaneously. At the end of this process, we obtain 30 crossings (15 crossings per day per each satellite) for each hemisphere. Daily maps are then drown by reducing data on a regular grid using a Gaussian kernel interpolation scheme.

4. Results

Figure 3 reports the results obtained for the Northern Hemisphere while those for the Southern Hemisphere are reported in Figure 4. Polar daily maps of both the first and the second scaling exponents for the time interval 16–22 March 2015 are shown together with the polar daily maps of RODI. All these quantities are represented as a function of QD-latitude and magnetic local time. The daily maps of the first-order scaling exponent (Figure 3, first column) in the interval [0.2, 0.8] give the opportunity to distinguish regions where the electron density fluctuations have a persistent character ($H > 0.5$ in red) from those characterized by an antipersistent one ($H < 0.5$ in blue). The antipersistent character seems to be a typical feature of high latitudes ($> 60°$) and the size of the region characterized by this antipersistent nature of the electron density fluctuations appears to increase approaching to and during the main phase of the geomagnetic storm. Conversely, the persistent character appears to be a typical feature of midlatitudes ($<60°$) where the values of H are everywhere greater than 0.5 regardless of the geomagnetic activity level. During the temporal evolution of the geomagnetic storm, the main feature is essentially the position of the profile defined by values of H equal to 0.5, that seems to follow the spatial and temporal evolution of the auroral zone during the selected period. The daily maps relative to the second-order scaling exponent (Figure 3, fifth column) show as the ionospheric polar regions are characterized by different values in the range between 0.5 and 1.8. Generally, the regions with an antipersistent character of the electron density fluctuations are characterized by values of the second-order scaling exponent less than 1. This means that the scaling exponent (β) of the power spectrum of the original signal is less than 2. Conversely, regions characterized by a more persistent behavior are usually associated with values $\xi(2)$ greater than 1 and consequently with values β greater than 2 at all analyzed scales. This suggests the existence of different scaling features, which depend on the latitude, MLT, and

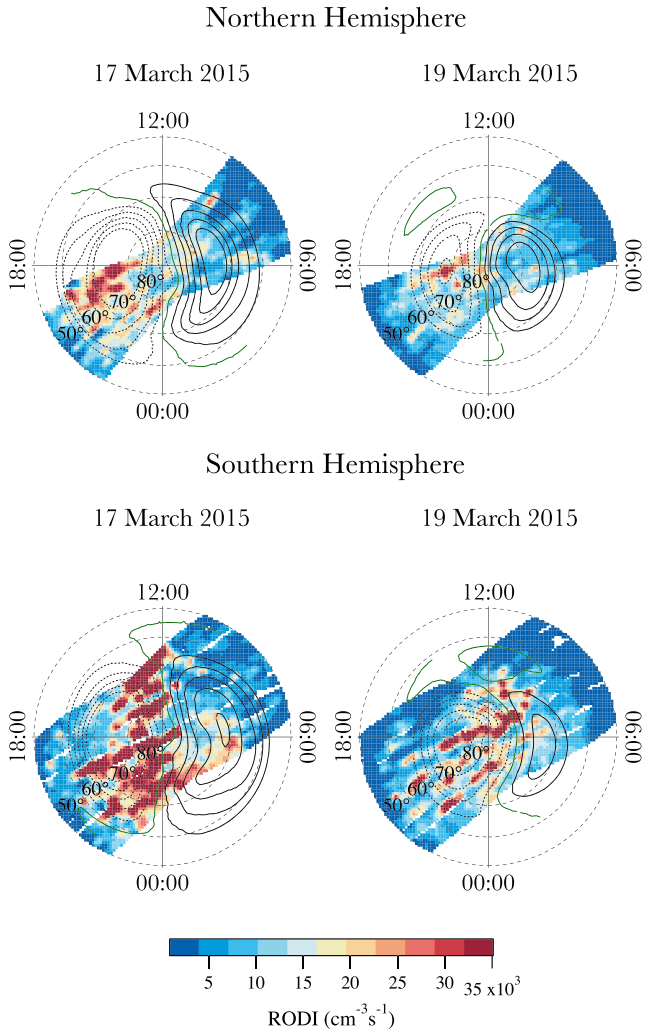

Figure 5. An example of comparison between satellite observations of RODI with SuperDARN polar potential maps obtained using the statistical convection model CS10. Data are reported as a function of MLT and QD latitude for two specific days for the Northern and Southern Hemispheres. The concentric circles represent contours of magnetic latitude, separated by intervals of 10°. The black contours are the ionospheric potential pattern, at 10 kV intervals. The dashed lines refer to negative values while the continuous lines to the positive ones.

geomagnetic activity level. Similar results are obtained for the Southern Hemisphere as it is shown in Figure 4.

The ionospheric regions marked by an antipersistent character of the electron density fluctuations and values of the second-order scaling exponent less than 1 seem to correspond to those regions where high values of RODI are recorded (see Figures 3 and 4, central column). To investigate the possible relationship between this index and the scaling features of the electron density fluctuations, the joint probability distributions between RODI and the first (Figures 3 and 4, second column) and second-order scaling exponents (Figures 3 and 4, fourth column) respectively, have been evaluated. High values of RODI are correlated with an antipersistent character ($H<0.5$) of the electron density fluctuations and values of the second-order scaling exponent $\xi(2)$ in the range from 0.5 to 0.7 (or β around 1.66). These features remain throughout the entire development of the storm and characterize both hemispheres. Low values of RODI are instead correlated with a persistent character ($H>0.5$) of the electron density fluctuations and values of second-order scaling exponent $\xi(2)$ greater than 1 (or $\beta>2$). The results suggest the existence of two different families of irregularities whose origin must be sought in different physical processes. We notice that the relative weight of the two families changes day after day during the analyzed period. The family of irregularities associated with a persistent character of the electron density fluctuations and values of the second-order scaling exponent greater than 1 becomes particularly visible during less disturbed days. It is also possible to notice a slight difference between the results obtained in the Northern and Southern Hemispheres. In the Southern Hemisphere this family of irregularities shows a greater joint probability with respect to the Northern Hemisphere. Conversely, the family of irregularities associated with an antipersistent character of the electron density fluctuations and values of the second-order exponent less than 1 seems to increase in the disturbed period, that is, during the main phase of the geomagnetic storm and the start of the recovery phase.

A more careful analysis of these two distinct families of irregularities shows that these are actually associated with different values of latitudes. High RODI values ($>10^{3.5}\,\mathrm{cm}^{-3}\,\mathrm{s}^{-1}$) characterized by electron density fluctuations with an antipersistent behavior and β around 1.66 can be found at high latitudes mainly in the auroral oval; low RODI values, characterized by electron density fluctuations with a persistent behavior and β larger than 2 ($\xi(2)>1$), can be found at midlatitudes below the auroral oval. As already underlined in the previous section, looking at the spatial distribution of the strongest and most pronounced irregularities, that is, of the highest values of RODI, we remark that they are essentially oriented in the day-night direction across the polar cap. These irregularities could be mainly attributed to dynamical processes including high-speed plasma convection (Cherniak & Zakharenkova, 2016). This suggests that the turbulent nature of the electron density fluctuations can be due to a Kelvin-Helmholtz instability and/or gradient drift instability in those regions characterized by strong shear flows. Now, for low-β plasmas (here $\beta=p_k/p_B$ refers to the ratio between kinetic plasma pressure p_k and magnetic pressure p_B) the expected turbulence is 2D and mainly fluid, generated by electrostatic fluctuations and characterized by a near $-5/3$ PSD, but the energy cascade is backward in the low-frequency range (Kintner & Seyler, 1985). In this framework, shear-flow-associated instabilities are the principal mechanism to generated turbulent fluctuations. However, we cannot exclude that the auroral particle precipitation could also be another source of the observed turbulent behavior mainly in the Northern Hemisphere where the high values of RODI tend to be concentrated along the auroral oval border. Looking at the values of the second-order scaling exponent $\xi(2)$ associated with the second RODI family

at values $<3 \times 10^3\ cm^{-3}\ s^{-1}$ one can note how this second family is characterized by $\xi(2) > 1$ (i.e., spectral scaling exponents higher than 2).These values are generally spatially located outer of the border of the convection zone, where different physical mechanisms could be responsible for the observed scaling features.

For more detailed study of the spatial distribution of the strongest and most pronounced irregularities during this geomagnetic storm, in the context of two-cell plasma convection, we compared RODI maps with Super Dual Auroral Radar Network (SuperDARN) polar potential maps obtained using the statistical convection model CS10 (Cousins & Shepherd, 2010). In this model high-latitude ionospheric convection patterns are obtained using average convection patterns derived from the SuperDARN measurements collected over many years for varying solar wind velocity, interplanetary magnetic field, and dipole tilt angle conditions. We have evaluated, for each day, the average values of these parameters and derived the corresponding average convection patterns independently for the Northern Hemisphere and Southern Hemisphere. Of course, these are average daily patterns that do not describe the real convection patterns characterizing the analyzed regions. The latter may indeed drastically change with varying interplanetary conditions. The average convection pattern, however, allows to understand where the irregularities described by the RODI are distributed.

Figure 5 reports a comparison between RODI and SuperDARN polar potential maps obtained using the statistical convection model CS10. Figure 5 reports the results obtained in both hemispheres in two different days, 17 and 19 March 2015, respectively. As we have hypothesized looking at the spatial distribution of the RODI values, the strongest and most pronounced irregularities during the geomagnetically disturbed days seem to follow the convection patterns. They are mainly localized along the convection patterns that travel across the polar cap from the dayside to the nightside. This result seems to support our hypothesis according to which the physical mechanisms responsible for the formation of high-latitude ionospheric irregularities characterized by high values of RODI can be both the gradient drift and the Kelvin-Helmholtz instability, while perhaps the low RODI values' family could be due to a different kind of turbulent/stochastic process.

5. Conclusions

The high-latitude ionosphere is extremely rich in plasma irregularities and fluctuations. They are due to a very long list of processes that depend mainly on the scale of interest. In the spatial scales from hundreds of kilometers down to some kilometers these irregularities partially depend on the interaction of the high-ionosphere with the various magnetospheric regions to which it is connected by magnetic field lines. Over the past two decades several studies focused on the characterization of plasma density irregularities and fluctuations at different spatial scales by using both ground-based observations and in situ measurements on-board LEO satellites. Our work has to be placed within this framework.

We have studied the nature of electron density fluctuations recorded on-board Swarm satellites at middle- and high-latitude regions in both hemispheres in order to investigate the self-similarity/affinity nature of the measured time series. We have thus looked for scaling invariance in the plasma density fluctuations (in terms of self-similarity) supporting the idea that turbulence might play a role in generating plasma irregularities. Based on this idea we have investigated a possible link between the observed scaling features and the electron density irregularities identified by RODI. Among the different irregularity parameters that can be derived from the plasma density measurements, RODI is indeed a measure of the electron density variations that shows a high correlation degree with the pattern of topside ionospheric irregularities (Zakharenkova et al., 2016).

So, the joint analysis of RODI and of the scaling features of electron density fluctuations recorded by Swarm A and B gave us the opportunity to locally analyze the small-scale (both spatial and temporal) fluctuations of electron density and investigate a possible relation between their properties and RODI in the ionospheric topside region. The study highlighted two families of plasma irregularities that seem to be associated with different physical properties. On one hand, there are plasma density variations associated with low values of RODI that are characterized by scaling properties not supporting the idea of a fluid and/or MHD turbulence as a source of these perturbations. These irregularities mainly occur in the midlatitude regions mainly below the auroral oval. On the other hand, there are plasma density variations associated with high RODI values ($> 10^{3.5}\ cm^{-3}\ s^{-1}$) and scale-invariant antipersistent fluctuations that are characterized by spectral

properties similar to those expected in the case of fluid and/or MHD turbulence. Indeed, in this case, the second-order scaling exponent to which the spectral feature is related, ranges from 0.5 to 0.8, supporting a near 5/3 spectral features (a quasi-Kolmogorov scaling) of the observed density fluctuations. These irregularities mainly occur at high latitudes in the auroral and polar cap regions and can be caused by direct particle precipitation and by dynamic plasma processes in the polar ionosphere involving turbulence. In other words they could be associated with a fluid/MHD plasma turbulence mechanisms generated by Kelvin-Helmholtz or shear flow instabilities. We note how the location of these irregularities seems to be associated with the convection pattern, that is, with the plasma transport across the polar cap as recently observed (Yang et al., 2016). Conversely, the second family of RODI values could be the consequence of a different turbulent and/or stochastic mechanism.

Our observations suggest that RODI, which is a proxy of ionospheric irregularities, cannot be generically considered as a proxy of the occurrence of ionospheric fluid/MHD turbulence. It is nevertheless true that its highest values ($> 10^{3.5}$ cm^{-3} s^{-1}) can give us information on the possible turbulent origin of the plasma irregularities. However, we cannot exclude that different turbulent/stochastic mechanism could be responsible for the occurrence of scaling (self-similar) features also in the case of RODI small values. This point deserves a more detailed analysis that calls for future work.

Data Availability Statement

Swarm data can be accessed online (http://earth.esa.int/swarm).

Acknowledgments

The results presented rely on data collected by two of the three satellites of the Swarm constellation. We thank the European Space Agency (ESA) that supports the Swarm mission. The authors kindly acknowledge V. Papitashvili and J. King at the National Space Science Data Center of the Goddard Space Flight Center for the use permission of 1 min OMNI data and the NASA CDAWeb team for making these data available (https://cdaweb.gsfc.nasa.gov/index.html/). The authors acknowledge financial support from European Space Agency (ESA contract N. 4000125663/18/I-NB-"EO Science for Society Permanently Open Call for Proposals EOEP-5 BLOCK4 (INTENS)). G. C. and G. B. have benefitted from discussions within the International Space Science Institute (ISEE) Team # 455 "Complex Systems Perspectives Pertaining to the Research of the Near-Earth Electromagnetic Environment".

References

Alessio, E., Carbone, A., Castelli, G., & Frappietro, V. (2002). Second-order moving average and scaling of stochastic time series. *European Physical Journal B*, *27*, 197–200.

Astafyeva, E., Zakharenkova, I., & Förster, M. (2015). Ionospheric response to the 2015 St. Patrick's day storm: A global multi-instrumental overview. *Journal of Geophysical Research: Space Physics*, *120*, 9023–9037. https://doi.org/10.1002/2015JA021629

Balasis, G., Daglis, I. A., Contoyiannis, Y., Potirakis, S. M., Papadimitriou, C., & Melis, N. S. (2018). Observation of intermittency-induced critical dynamics in geomagnetic field time series prior to the intense magnetic storms of March, June, and December 2015. *Journal of Geophysical Research: Space Physics*, *123*, 4594–4613. https://doi.org/10.1002/2017JA025131

Balasis, G., Daglis, I. A., Kapiris, P., Mandea, M., Vassiliadis, D., & Eftaxias, K. (2006). From pre-storm activity to magnetic storms: A transition described in terms of fractal dynamics. *Annales de Geophysique*, *24*, 3557–3567.

Basu, S., Basu, S., MacKenzie, E., Coley, W. R., Hanson, W. B., & Lin, C. S. (1984). F-region electron density irregularity spectra near auroral acceleration and shear regions. *Journal of Geophysical Research*, *89*, 5554–5564. https://doi.org/10.1029/JA089iA07p05554

Basu, S., Basu, S., MacKenzie, E., Fougere, P. F., Coley, W. R., Maynard, N. C., et al. (1988). Simultaneous density and electric field fluctuation spectra associated with velocity shears in the auroral oval. *Journal of Geophysical Research*, *93*, 115–136. https://doi.org/10.1029/JA093iA01p00115

Carbone, A., Castelli, G., & Stanley, H. E. (2004). Time-dependent Hurst exponent in financial time series. *Physica A*, *344*, 267–271.

Cerisier, J. C., Berthelier, J. J., & Beghin, C. (1985). Unstable density gradients in the high-latitude ionosphere. *Radio Science*, *20*, 755–761.

Chaston, C. C. (2008). The turbulent Alfvénic aurora. *Physical Review Letters*, *100*(175003).

Cherniak, I., & Zakharenkova, I. (2016). High–latitude ionospheric irregularities: Differences between ground– and space–based GPS measurements during the 2015 St. Patrick's Day storm. *Earth Planets and Space*, *68*, 136. https://doi.org/10.1186/s40623-016-0506-1

Cherniak, I., Zakharenkova, I., & Redmon, R. J. (2015). Dynamics of the high-latitude ionospheric irregularities during the 17 March 2015 St. Patrick's Day storm: Ground–based GPS measurements. *Space Weather*, *13*, 585–597. https://doi.org/10.1002/2015SW001237

Cousins, E. D. P., & Shepherd, S. G. (2010). A dynamical model of high–latitude convection derived from SuperDARN plasma drift measurements. *Journal of Geophysical Research*, *115*, A12329. https://doi.org/10.1029/2010JA016017

De Michelis, P., Consolini, G., & Tozzi, R. (2015). Magnetic field fluctuation features at Swarm's altitude: A fractal approach. *Geophysical Research Letters*, *42*, 3100–3105. https://doi.org/10.1002/2015GL063603

De Michelis, P., Consolini, G., Tozzi, R., & Marcucci, M. F. (2017). Scaling features of high latitude geomagnetic field fluctuations at Swarm altitude: Impact of IMF orientation. *Journal of Geophysical Research: Space Physics*, *122*, 10,548–10,562. https://doi.org/10.1002/2017JA024156

Dyrud, L., Krane, B., Oppenheim, M., Pécseli, H. L., Trulsen, J., & Wernik, A. W. (2008). Structure functions and intermittency in the ionosphere plasma. *Nonlinear Processes in Geophysics*, *15*, 847.

Dyson, P. L., Hanson, J. P., & McClure, W. B. (1974). In situ measurements of the spectral characteristics of *F* region ionospheric irregularities. *Journal of Geophysical Research*, *79*, 1497–1502. https://doi.org/10.1029/JA079i010p01497

Earle, G. D., Kelley, M. C., & Ganguli, G. (1989). Large velocity shears and associated electrostatic waves and turbulence in the auroral *F* region. *Journal of Geophysical Research*, *94*(A11), 15,321–15,333. https://doi.org/10.1029/JA094iA11p15321

Giannattasio, F., De Michelis, P., Consolini, G., Quattrociocchi, V., Coco, I., & Tozzi, R. (2019). Characterising the electron density fluctuations in the high-latitude ionosphere at Swarm altitude in response to the geomagnetic activity. *Annals of Geophysics*, *62*(4), GM453. https://doi.org/10.4401/ag-7790

Gjerloev, J. W., Ohtani, S., Iijima, T., Anderson, B., Slavin, J., & Le, G. (2011). Characteristics of the terrestrial field-aligned current system. *Annales de Geophysique*, *29*, 1713–1729.

Golovchanskaya, I. V., & Kozelov, B. V. (2010). On the origin of electric turbulence in the polar cap ionosphere. *Journal of Geophysical Research*, *115*, A09321. https://doi.org/10.1029/2009JA014632

Golovchanskaya, I. V., Ostapenko, A. A., & Kozelov, B. V. (2006). Relationship between the high-latitude electric and magnetic turbulence and the Birkeland field-aligned currents. *Journal of Geophysical Research*, *111*, A12301. https://doi.org/10.1029/2006JA011835

Grach, S. M., Sergeev, E. N., Mishin, E. V., & Shindin, A. V. (2016). Dynamic properties of ionospheric plasma turbulence driven by high-power high-frequency radiowaves. *Physics-Uspekhi*, *59*, 1091.

Heppner, J. P., Liebrecht, M. C., Maynard, N. C., & Pfaff, R. F. (1993). High-latitude distributions of plasma waves and spatial irregularities from DE2 alternating current electric field observations. *Journal of Geophysical Research*, *98*, 1629–1652.

Hurst, H. (1956). Methods of using long-term storage in reservoirs. *ICE Proceedings*, *5*(704), 519–543.

Jin, Y., Spicher, A., Xiong, C., Clausen, L. B. N., Kervalishvili, G., Stolle, C., & Miloch, W. J. (2019). Ionospheric plasma irregularities characterized by the Swarm satellites: Statistics at high latitudes. *Journal of Geophysical Research: Space Physics*, *124*, 1262–1282. https://doi.org/10.1029/2018JA026063

Kintner, P. M. Jr., & Seyler, C. E. (1985). The status of observations and theory of high latitude ionosphere and magnetospheric plasma turbulence. *Space Science Reviews*, *41*, 91.

Knudsen, D. J., Burchill, J. K., Buchert, S. C., Eriksson, A. I., Gill, R., Wahlund, J.-E., et al. (2017). Thermal ion imagers and Langmuir probes in the Swarm electric field instruments. *Journal of Geophysical Research: Space Physics*, *122*, 2655–2673. https://doi.org/10.1002/2016JA022571

Kozelov, B. V., & Golovchanskaya, I. V. (2006). Scaling of electric field fluctuations associated with the aurora during northward IMF. *Geophysical Research Letters*, *33*, L20109. https://doi.org/10.1029/2006GL027798

Laundal, K. M., & Richmond, A. D. (2016). Magnetic coordinate systems. *Space Science Reviews*, *206*, 27–59. https://doi.org/10.1007/s11214-016-0275-y

Mounir, H., Berthelier, A., Cerisier, J. C., Lagoutte, D., & Beghin, C. (1991). The small-scale turbulent structure of the high latitude ionosphere-Arcad-Aureol-3 observations. *Annales Geophysicae*, *9*, 725.

Nava, B., Rodrìguez-Zuluaga, J., Alazo-Cuartas, K., Kashcheyev, A., Migoya-Oruè, Y., Radicella, S. M., et al. (2016). Middle– and low–latitude ionosphere response to 2015 St. Patrick's Day geomagnetic storm. *Journal of Geophysical Research: Space Physics*, *121*, 3421–3438. https://doi.org/10.1002/2015JA022299

Olsen, N., Friis-Christensen, E., & Floberghagen, R. (2013). The Swarm Satellite Constellation Application and Research Facility (SCARF) and Swarm data products. *Earth, Planets and Space*, *65*, 1.

Pécseli, H. (2016). Turbulence in the ionosphere. In H. Pécseli (Ed.), *Chapter 24 of "Low frequency waves and turbulence in magnetized laboratory plasmas and in the ionosphere"*. Bristol, UK: IOP Science.

Peng, C. K., Buldyrev, S. V., Havlin, S., Simons, M., Stanley, H. E., & Goldberger, A. L. (1994). Mosaic organization of DNA nucleotides. *Physical Review. E, Statistical Physics, Plasmas, Fluids, and Related Interdisciplinary Topics*, *49*, 1685.

Poppe, B. B. (2000). New scales help public, technicians understand space weather. *Eos, Transactions American Geophysical Union*, *81*(29), 322–328. https://doi.org/10.1029/00EO00247

Prölss, G. W. (1987). Storm–induced changes in the thermospheric composition at middle latitudes. *Planetary and Space Science*, *35*, 807–811. https://doi.org/10.1016/0032–0633(87)90041–9

Ram, S. T., Yokoyama, T., Otsuka, Y., Shiokawa, K., Sripathi, S., Veenadhari, B., et al. (2015). Duskside enhancement of equatorial zonal electric field response to convection electric fields during the St. Patrick's day storm on 17 March 2015. *Journal of Geophysical Research: Space Physics*, *121*, 538–548. https://doi.org/10.1002/2015JA021932

Ramsingh, S., Sreekumar, S., Banola, S., Emperumal, K., Tiwari, P., & Kumar, B. S. (2015). Sripathi Low-latitude ionosphere response to super geomagnetic storm of 17/18 March 2015: Results from a chain of ground-based observations over indian sector. *Journal of Geophysical Research: Space Physics*, *120*, 10,864–10,882. https://doi.org/10.1002/2015JA021509

Spicher, A., Miloch, W. J., Moen, L. B. N., & Clausen, J. I. (2015). Plasma turbulence and coherent structures in the polar cap observed by the ICI-2 sounding rocket. *Journal of Geophysical Research: Space Physics*, *120*, 10,959–10,978. https://doi.org/10.1002/2015JA021634

Tam, S., Chang, W. Y., Kintner, P. M., & Klatt, E. (2005). Intermittency analyses on the SIERRA measurements of the electric field fluctuations in the auroral zone. *Geophysical Research Letters*, *32*, L05109. https://doi.org/10.1029/2004GL021445

Weimer, D. R., Goertz, C. K., & Gurnett, D. A. (1985). Auroral zone electric fields from DE 1 and 2 at magnetic conjunctions. *Journal of Geophysical Research*, *90*, 7479–7494. https://doi.org/10.1029/JA090iA08p07479

Yang, S.-G., Zhang, B.-C., Fang, H.-X., & Kamide, Y. (2016). New evidence of dayside plasma transportation over the polar cap to the prevailing dawn sector in the polar upper atmosphere for solar-maximum winter. *Journal of Geophysical Research: Space Physics*, *121*, 5626–5638. https://doi.org/10.1002/2015JA022171

Zakharenkova, I., Astafyeva, E., & Cherniak, I. (2016). GPS and in situ Swarm observations of the equatorial plasma density irregularities in the topside ionosphere. *Earth, Planets and Space*, *68*, 120. https://doi.org/10.1186/s40623-016-0490-5